J. Min. Metall. Sect. B-Metall. 47 (1) B (2011) 37 - 44

Journal of Mining and Metallurgy

PHYSICAL AND MATHEMATICAL MODELING OF INCLUSION REMOVAL WITH GAS BOTTOM-BLOWING IN CONTINUOUS CASTING TUNDISH

M. J. Zhang#, H. Z. Gu, A. Huang, H. X. Zhu and C. J. Deng

Wuhan University of Science and Technology, The Hubei Province Key Laboratory of Refractories and Ceramics, Wuhan 430081, China

(Received 22 August 2010; accepted 24 February 2011)

Abstract

Gas blowing at the bottom of tundish is an efficient metallurgy technique in clean steelmaking and has been widely concerned. In this paper, spherical alumina particles were selected to model inclusions, 1:3 scale model was utilized, the removal efficiency of inclusions with the gas bottom-blowing in the tundish was studied by physical and mathematical modeling. The mathematical model is validated by comparing the predicted and measured residence time distributions and dye flow patterns of tracer. The results show that while the removal efficiency of large size particles has no obvious changes, the gas bottom-blowing has great contribution to the removal of small particles.

Keywords: Tundish; Inclusion removal; Gas blowing, Modeling.

1. Introduction

The tundish is the last reactor before the solidification of molten steel in the continuous casting. A variety of methods have been used in the tundish to control steel flow, such as dams, weirs and turbulence inhibitor (TI) [1-3]. The use of gas curtain to control steel flow in tundishes has been an useful approach to attain high steel quality [4-6]. The gas curtain works as dams and weirs to control the fluid flow [7]. At the same time, gas bubbles capture inclusions during the floating process to the metal-slag interface [8-9]. R.D. Morales et al [6, 10] performed water-modeling experiment using a 2/5 scale of a one-strand slab tundish of a Brazilian caster. They found that small flow

Corresponding author: major6886@gmail.com

DOI:10.2298/JMMB1101037Z

rates of gas injection (246 Ncm^3/min) through a gas curtain improved the fluid flow by enhancing the plug flow volume fraction. The high flow rates led to a thermal homogenization in two separated cells of flow located at each side of the gas curtain. Industrial experiment indicated that argon bubbling in the tundish was helpful to decrease the population of inclusions in the final product [11,12].

Many researches have verified that large inclusions (>50μm) can be removed by controlling the molten steel flow [13, 14]. With the widely used of computer simulation in metallurgy process [15, 16], J.P. Rogler et. al. [5, 8] predicted the inclusion removal efficiency by gas bubbling using mathematical model. Then, they studied the effects of bubbling gas flow rate, inclusion particle size and bubble size. They also found that gas bubbling was a high efficient means for the enhancement of inclusion removal in a tundish. Wang Laihua and coworkers [17] discussed the inclusion removal mechanism by bubbles and claimed that the main contribution of bubbles is to remove small inclusions. So the main objective of this work is to study the possibility of removal of small inclusions by gas bottom-blowing in the tundish using both water modeling and mathematical modeling.

2. Physical model description

According to the similarity theory, liquid steel being replaced by water, argon being replaced by air, a 1/3 scale tundish model made of clear plastic was built with the internal geometric dimensions shown in Figure 1. Froude similarity was used in order to satisfy the dynamic similarity: $Fr_m = Fr_p$. A turbulent inhibitor (TI) was established on the tundish bottom, just below the tip of the ladle shroud. Figure 2 shows the internal geometric dimensions of this inhibitor. This prototype tundish and turbulence inhibitor were used in Wuhan Iron and Steel (Group) Corporation. Two porous plugs were symmetrically installed on the bottom of tundish at position located 400mm from the inlet axis. The scheme of the experimental setup was shown in Figure 3. In order to simulate the gas bubbling curtain, porous plugs were prepared. The average pore diameter and permeability of porous plugs were controlled to make them similar to the industrially used porous

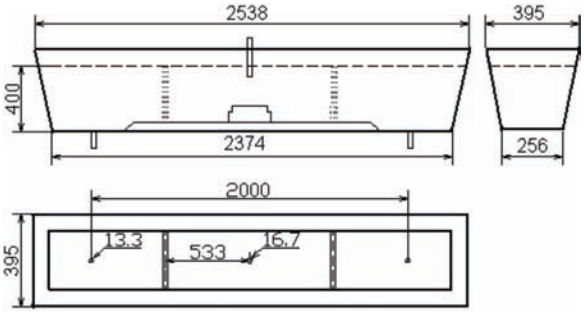

Fig.1 Geometric dimensions of water model tundish

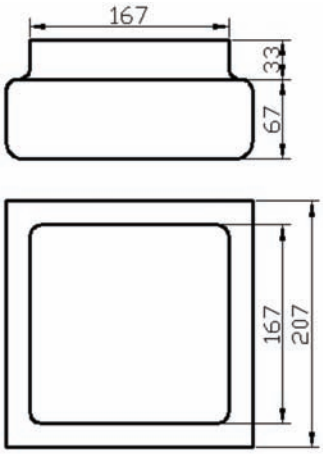

Fig. 2 Geometric dimensions of turbulence inhibitor

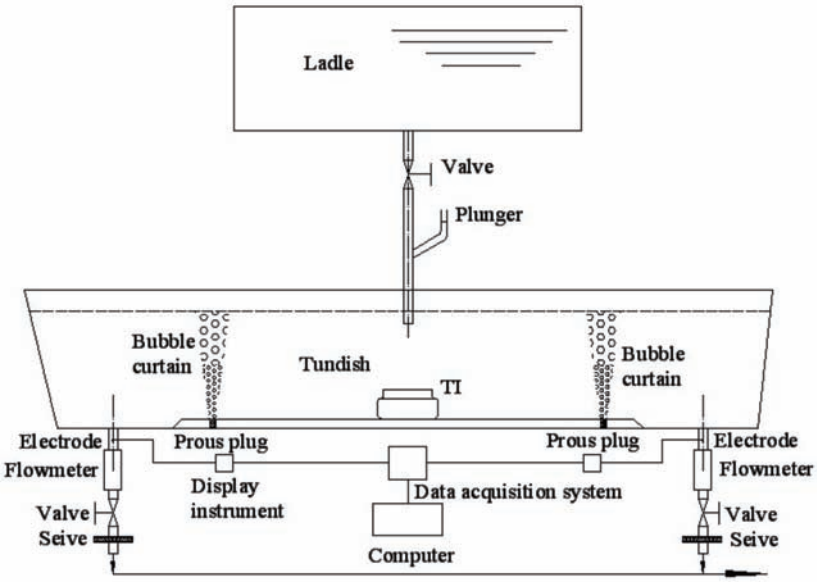

Fig. 3 Schematic diagram of the water model

refractories. Dimensions of the plug are shown in Figure 4. The gas flow rate was controlled with a rotameter type flow meter with a capacity from 0 to 0.3m^3/h at room temperature. In order to collect the particles, two 400 mesh sieves were placed at each exit of water flowing as shown in Figure 3. Residence Time Distribution (RTD) curves were determined through the typical pulse input signal technique using saturated sodium chloride solution [18]. Dye flow patterns were observed through the typical pulse input signal technique using red ink as dye tracer [19].

The choice of particle used in the physical modeling is an important element in the simulation of the separation behavior of typical inclusions in liquid steel such as alumina. In this experiment, spherical alumina particles were used to simulate the inclusions. The density of spherical alumina particles is 980 kg/m^3. A mixture of kerosene and engine oil at the mass proportion of 89/11 served as an analogue for refining slag on the free surface. The density of oil mixture is 0.8085kg/m^3.

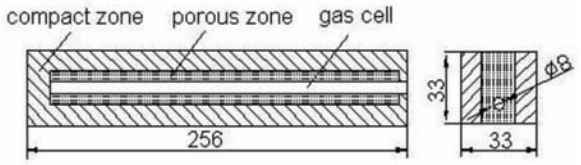

Fig. 4 Schematic of gas curtain bricks for water model

To define an initial particle size distribution for the tests, the initial inclusion size distribution in molten steel of tundish reported in reference [13], (table 1) was used. It is difficult to find particles with the same density ratio to the real situation, i.e.

$$\frac{\rho_{\mathrm{inc,m}}}{\rho_{\mathrm{w}}} \neq \frac{\rho_{inc,p}}{\rho_{\mathrm{st}}} \qquad ...(1)$$

Where $\rho_{\mathrm{inc,p}}$ is particle density of prototype model and is assumed as 3500 kg/m^3; $\rho_{\mathrm{inc,p}}$ is particle density of the water model and is 980 kg/m^3. The subscripts inc, st and w denote inclusion, molten steel and water respectively; the subscripts m and p

denote water model and prototype model respectively.

Sahai and Emi [20] have analyzed the similarity of particles. Assuming that the kinematical viscosity of water at room temperature is nearly same as that of steel at 1873K, equation (2) can be used for the model inclusion size with different density ratios.

$$\frac{R_{\mathrm{inc,m}}}{R_{\mathrm{inc,p}}} = \lambda^{0.25}\left[\left(1-\frac{\rho_{inc,p}}{\rho_{\mathrm{st}}}\right)\Big/\left(1-\frac{\rho_{\mathrm{inc,m}}}{\rho_{\mathrm{w}}}\right)\right]^{0.5} \quad ...(2)$$

Where R is radius of inclusions,μm; λ is scale factor.

Spherical alumina particles sieving was carried out using standard ASTM sieves to produce six five ranges of particles for experimentation shown in Table 1.

After water and bubble flow reached a steady state, a total amount of 200g of mixed size inclusions was injected into the tundish with a plunger placed on the shroud as shown in Figure 3.

After some time, the inclusions floated up to the surface and adhered to the mixed oil. Particles were collected for the time which is as three times as the tundish mean residence time. During this time, all particles either had separated from the tundish bath or had been collected in the particle collector. At the end of each experiment, the particle collectors were removed and dried at 100 ºC. After screening test, the weight of different size particles were measured after each experiment. The average mass of particles for three times experiment was calculated. The removal efficiency of different size inclusions ($\eta_{\mathrm{f.i}}$) was calculated as formula (3).

$$\eta_{f,i}(\%) = \frac{m_0 - m_{out,i}}{m_0} \times 100 \quad ...(3)$$

Where m_0 is the amount of particles injected through inlet, kg; $m_{\mathrm{out},\ i}$ is the amount of particles of the specified size i collected at exit, kg.

3. Mathematical modeling

The liquid and gas flow in the tundish was modeled using Eulerian-Eulerian model. The water is considered as the primary phase and gas as the secondary phase. Each phase has its own set of continuity and momentum equations. Coupling is achieved through an empirical inter-phase drag between water and air bubbles. The standard two-equation k-ε turbulence model is chosen for the liquid phase. The detail equations and boundary conditions are same as references [20, 21]. The gas flow through the permeable brick was modeled using porous media model [22, 23]. The viscous resistance factor and inertial resistance factor of gas flow in the brick were acquired by the method for measuring permeability of refractory products [24]. The equation for RTD is a normal species transportation equation [25]. The inclusions were removed mainly by three mechanisms: floating to the free surface due to Stokes floatation and adopted by slag; adhesion to the tundish wall and removed by bubbles.

Table 1 the initial inclusion size distribution for water model

Protype model particle size/[μm]	10~20	20~36	36~50	50~100	100~
Water model particle size/[μm]	44~89	89~150	150~200	200~500	500~
Composition /[%]	27.4	50.3	12.8	2.8	1.2

Inclusion trajectories were calculated using the discrete phase model (DPM) under the following assumptions.

(1) Inclusions are assumed to be spherical and the density is the same as the spherical alumina particles. The size distribution of inclusion particles is shown in table 1.

(2) The size of inclusions is so small that the effect of inclusion on flow of water is negligible.

(3) The inclusions were chaotically distributed at the inlet surface and injected into the tundish at the rate of water inlet velocity.

(4) At the top surface, ideal absorption was assumed. At the tundish wall, only a part of inclusions were adopted and the adhesion probability was calculated as formula (4).

$$P_{wa}=\exp(-0.287\tau_w/\tau_2) \quad ...(4)$$

Where τ_w is shear stress which can be calculated according to the fluid flow; τ_2 is critical shear stress at the wall surface and can be calculated as reference [26].

(5) The overall removal probability by bubbles was calculated according to the formula (5).

$$P_B = P_C\ P_A\ (\ 1\text{-}P_D\ ) \quad (5)$$

Where P_A, P_C and P_D represent the probability of adhesion, collision and detachment, respectively. For very small inclusions, the detachment probability(P_D) from the bubbles is insignificant and can be set as zero. P_A and P_C can be calculated according to Yoon and Lutrell model [27].

After getting the steady fluid flow, inclusions were injected into the tundish from the inlet. Ten simulations for each case of inclusions trajectories were performed including 1200 particles. The trajectory of each particle was calculated. The total number of injected particles was written as N_t, the number of absorbed particles for different size by the walls was written as $N_{a,i}$, the number of particles for different size floated to the free surface was written as $N_{f,i}$. The different size inclusion removal efficiency can be calculated as:

$$\eta_{t,i} = (\ N_{f,i} + N_{a,i}\ ) / N_t \quad ...(5)$$

4. Results and discussion

4.1. Validation of the model

Figure 5 shows the comparisons of RTD curves between mathematical modeling and water modeling. The comparisons of dye flow patterns of tracer are shown as Figure 6, where Figure 6 (a) shows the results of water modeling, Figure 6 (b) shows the results of mathematical modeling.

In predicting the response time, peak time and the overall trend of RTD curves consist well with the values simulated by mathematical modeling as shown in Figure 5.

A mass transfer experiment recorded in a

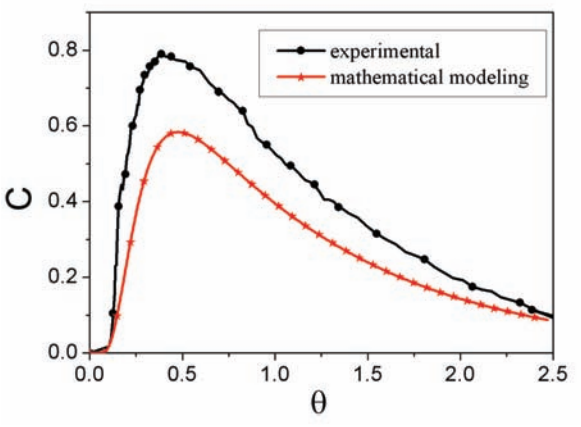

Fig. 5 RTD curves predicted by water modeling and numerical modeling

digital video image is shown in Figure 6 (a). After 3 seconds of the tracer injection, the tracer is mainly confined to the inlet zone including turbulence regions. After 30 seconds of the tracer injection, the tracers reached bubble curtain zones and flowed upwards with the floating bubbles and then spread along the free surface. After 90 seconds of the tracer injection, the tracers reached the outlet. These results agreed well with those obtained by mathematical modeling as shown in Figure 6 (b).

4.2. Trajectories of inclusion particles

Figure 7 shows the pathlines of different sizes of particles in the gas bubbling tundish and without gas bubbling tundish.

It can be seen from Figure 7 almost all 50μm and 100μm inclusion particles flow to the outlet in the tundish only established with TI. When gas was blowing from the bottom, some 100μm inclusion particles without gas bubbling floated to the surface and were removed by slag. Figure 8 shows the inclusion removal efficiency of different sizes of particles in different tundishes using water modeling. The results obtained from mathematical modeling are almost same as the water modeling.

It can be seen from Figure 8, the removal efficiency of total particles increased from 41% to about 70% with gas bottom-blowing in tundish. For the large size particles (500μm ~), there was no significant influence on removal efficiency with gas

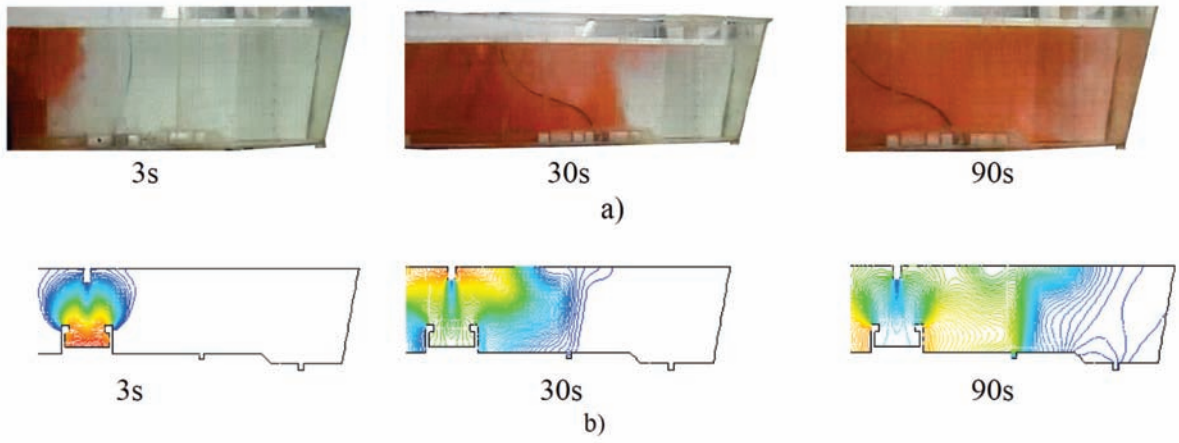

Fig. 6 Dye flow patterns in the tundish with TI and bottom gas blowing a-measured in water modeling, b- computed using mathematical modeling

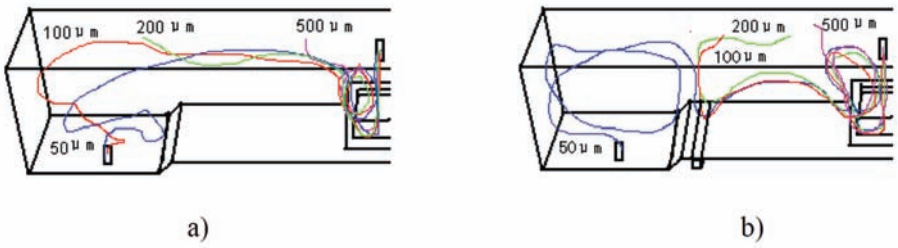

Fig. 7 Pathlines of inclusion particles a- with gas bubbling, b- without gas bubbling

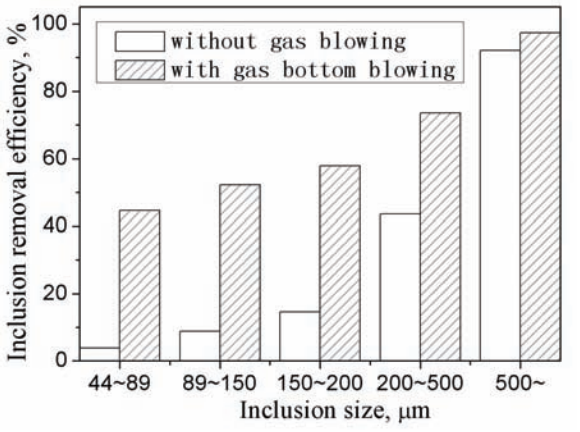

Fig.8 Comparison of removal efficiency of different sizes of particle

bottom-blowing. In the case of small size particles (~200μm), the removal efficiency was obviously enhanced. So, the main contribution of gas bubbling is removing the micro-inclusions.

5. Conclusions

The efficiency for promotion removals of inclusions in the bottom gas blowing tundish were studied using physical and mathematical modeling. The main conclusions derived from this study are as follows.

(1) According to the similarity theory, water, air and spherical alumina particles were selected as analogue media, RTD curves and inclusions removal efficiency in the tundish were modeled.

(2) Using Eulerian-Eulerian and DPM model, the liquid-gas flow, inclusion trajectories and the removal efficiency were numerically calculated. The results agreed well with those obtained from the water modeling.

(3) Almost all large size particles floated up to the surface and were removed whether there was gas bottom-blowing in the tundish or not. With gas bottom-blowing in the tundish, some small size particles adhered to the bubbles and floated up to the surface when encountering the gas bubbles curtain.

Acknowledgments

This work is supported by the State Key Development Program for Basic Research of China (2009CB62600) and Natural Science Foundation of Hubei Province of China(2009CDZ010).

References

[1] L. Zong, B. Li, Y. Zhu, R. Wang, We.Wang and X. Zhang. ISIJ Intern., 47 (1) (2007) 88.

[2] K. Pardeep, P. Srinivasa and A. Dewan. ISIJ Intern., 48 (2) (2008) 154.

[3] P. Gardin, M. Brunet, J.F. Domgin and K. Pericleous. Appl. Math. Modeling, 26(2002)323

[4] L. Zhang and S. Taniguchi: Intern. Mater. Rev., 45 (2000) 59.

[5] J.P. Rogler, L.J.Heaslip and M. Mehrvar. Can. Metall. Q., 44 (2005) 357.

[6] A. Ramos-Banderas and R.D.Morales: ISIJ Intern., 43 (5) (2003) 653.

[7] L. Zhang and S. Taniguchi: ISS Transl, Iron & Steelmaker, 28 (2001) 55.

[8] J.P. Rogler, L.J. Heaslip and M. Mehmvar. Can. Metall. Q., 43 (2004) 407.

[9] E. Koch, A. Niedermayr and H.-P. Narzt et al: Bhm., 140 (1995) 470.

[10] A.Vargas-Zamora, R.D. Morales, M. Diaz-Cruz, J. Palafox-Ramos and J. Dej. Barreto-Sanddval: Metall. Mater. Trans. B, 35 (2004) 247.

[11] H. Ao, T. Xiaolin and G. Huazhi et al. Steelmaking, 25 (2009) 42. (in Chinese)

[12] T. Liqun, J. Maofa and Z. Miaoyong et al. Iron and Steel, 41 (2006) 32.

[13] A. Kumar S. and Y. Sahai. ISIJ Intern., 33 (5) (1993) 556.

[14] Y. Wang, G. Wen, P. Tang, Mingmei Zhu, Y. Chen and W. Song. Journ. Univ. Sci. Tech. Beijing, 14(2007) 22. (in Chinese)

[15] W. Gong, L. Zhang, M. Ode, H. Murakami et al. J. Min. Metall. Sect. B-Metall. 46 (2) B (2010) 153.

[16] M.J. Bu, P.S. Wang, H.H. Xu et al. J. Min. Metall. Sect. B-Metall. 46 (2) B (2010) 181.

[17] W. Laihua, H.-G. Lee and P.r Hayes. ISIJ Intern., 36 (1) (1996) 17.

[18] D. Mazumdar and R.I.L. Gutrie. ISIJ Intern., 39 (5) (1999) 524.

[19] J.-H. Zong, K.-W. Yi and J.-K. Yoon. ISIJ Intern., 39 (2) (1999) 139.

[20] Y.Sahai and T.o Emi. ISIJ Intern., 36 (9) (1996) 1166.

[21] M.J. Zhang. Phd. thesis, Wu han University of Sci. & Tech., 2006. (in Chinese)

[22] M.J. Zhang, H.Gu, A. Huang: Journ. Iron and Steel Res, Intern., 20 (2008) 13. (in Chinese)

[23] S. Ergun: Chem. Eng. Prog., 48 (1952) 89.

[24] M.J. Zhang, H. Wang, H. Gu and A. Huang. Key Eng. Mater., 368-372 (2008) 1155.

[25] A. Kumar, D. Mazumdar and S.C. Koria. ISIJ Intern., 48 (2008) 38.

[26] B.W. Zhang. Phd. thesis, Shanghai University, 2003.(in Chinese)

[27] R.H. Yoon and G.H. Luttrell. Min. Processing and Extractive Metall. Rev., 5 (1989) 450.